International Journal of Nanomedicine

Dovepress
Taylor & Francis Group

Open Access Full Text Article

ORIGINAL RESEARCH

Fabrication of Nano-Silver Composite Using *Amomum longiligulare* Fruit Polysaccharides and Their Biological Activities

Yong Lian[1,*], Ning Ma[2,*], Qianying Cheng[1,*], Mingquan Luo[1], Zhen Xu[1], Fei He[1], Xiaomei Zhou[1], Ying Zhang[1], Dejun Jin[1], Yidan Kong[1], Yong Wang[1], Na Wei[1]

[1]Hainan Provincial Key Laboratory of R&D on Tropical Herbs, Engineering Research Center of Tropical Medicine Innovation and Transformation of Ministry of Education, International Joint Research Center of Human-Machine Intelligent Collaborative for Tumor Precision Diagnosis and Treatment of Hainan Province, School of Pharmacy, Hainan Medical University, Haikou, 571199, People's Republic of China; [2]Reproductive Medical Center, Hainan Women and Children's Medical Center, Haikou, Hainan Province, People's Republic of China

*These authors contributed equally to this work

Correspondence: Na Wei; Yong Wang, Hainan Provincial Key Laboratory of R&D on Tropical Herbs, School of Pharmacy, Hainan Medical University, Haikou, 571199, People's Republic of China, Email weina-0613@163.com; wangyong1982_2004@163.com

Purpose: Study aims to optimize the synthesis conditions for silver nanoparticle composites [ALP(D)-AgNPs] using a rapid and environmentally friendly method and investigate the antioxidant, antibacterial, and anticancer activities of the fabricated composite.

Methods: The polysaccharide component ALP-D was extracted and purified from the fruits of *Amomum longiligulare* and subsequently used for further experiments. The structure of ALP-D was characterized by FT-IR, monosaccharide composition and molecular weight.The optimal conditions for the green synthesis of silver nanoparticles using ALP-D were determined through single-factor experiments. The synthesized silver nanoparticles were characterized by UV-Vis spectroscopy, FT-IR, DLS, HRTEM and XRD. Finally, the in vitro antioxidant activity, antibacterial activity and anticancer activity of the nano-silver composite were evaluated.

Results: Single-factor experiments identified the optimal synthesis conditions for ALP(D)-AgNPs as a reaction time of 180 min, a temperature of 100 °C, and a 10:1 volume ratio of silver nitrate to ALP-D. The free radical scavenging activity of ALP(D)-AgNPs against DPPH and ABTS was significantly enhanced compared with that of ALP-D. The minimum inhibitory concentration (MIC) values of ALP(D)-AgNPs against E coli and B subtilis were 31.25 μg/mL, while the MIC value against S aureus was 62.5 μg/mL. The minimum bactericidal concentration (MBC) values of ALP(D)-AgNPs were 125 μg/mL for E coli, B subtilis, and S aureus. The IC50 values of ALP(D)-AgNPs on the MDA-MB-231, HepG2, Caco-2, and C6 cancer cell lines were 14.72 ± 0.23, 8.19 ± 0.65, 22.73 ± 3.01, and 15.77 ± 2.91 μg/mL, respectively.

Conclusion: In summary, we have identified a novel material for the green synthesis of silver nanoparticles. The results show the ALP(D)-AgNPs synthesized using the new material ALP-D exhibit excellent stability and dispersibility. Furthermore, the biological activity reveals that ALP(D)-AgNPs possess notable antioxidant, antibacterial, and cancer-suppressing activities.

Keywords: ALP-D, ALP(D)-AgNPs, antioxidant activity, antibacterial activity, anticancer activity

Introduction

The Chinese Pharmacopoeia (2020 edition) stipulates *Amomi Fructus* as the dry and ripe fruits of *Amomum villosum Lour, Amomum villosum Lour.var.xanthioides* T.L.Wu et Senjen or *Amomum longiligulare* T.L.Wu, which belong to the cardamom plants of the Zingiberaceae family.[1] *Amomum longiligulare* T.L.Wu is mainly cultivated in Chengmai, Lingshui, and other counties in Hainan, China, where it is recognized as a unique variety with a history of use more than 1300 years.[2] The fruits of *A. longiligulare* serve as both a traditional medicinal and edible material. While previous studies have primarily focused on small molecule drugs, research on polysaccharide macromolecules derived from the fruits of *A. longiligulare* remains limited. However, modern investigations have increasingly highlighted polysaccharides

Received: 5 November 2024
Accepted: 29 January 2025
Published: 12 February 2025

due to their non-toxicity, biodegradability and excellent biocompatibility. These advantages have facilitated the application of polysaccharides across various industries, including food and biomedicine.[3]

Silver nanoparticles are widely used in biomedical applications due to their antibacterial, antioxidant, and anticancer properties.[4] However, the traditional synthesis methods for silver nanoparticles can lead to environmental pollution, and the organic reagents employed are often toxic to humans.[5] Consequently, their application in the medical field is limited. This underscores the urgent need for new, environmentally friendly synthesis method for silver nanoparticles. Nowadays, to address the toxicity associated with conventional techniques, researchers have recently developed rapid and green synthesis methods for nanoparticles that utilizes biological extracts. Various sources, including bacteria,[6] fungi,[7] algae,[8] plants,[9] yeast[10] and other extracts have been employed to prepare silver nanoparticles.

Recent studies have demonstrated that silver nanoparticles can be synthesized using plant polysaccharides in an environmentally friendly manner, employing a one-step process that does not require the addition of organic reagents.[11] Moreover, it has been shown that polysaccharides not only prevent the aggregation of silver nanoparticles but also reduce the toxicity of silver nanoparticles.[12] This process offers several advantages, including cost-effectiveness, environmental protection and non-toxicity.[13,14] For example, Ma et al[15] extracted soluble soybean polysaccharides from *soybeans* and successfully prepared stable nano-silver particles with an average particle size of 2.9 ± 0.7 nm, which exhibited notable antibacterial activity. Similarly, Yang et al[16] utilized *pachyman* to synthesize nano-silver particles that also showed significant antibacterial properties. Furthermore, Li et al[17] reported that PPP-AgNPs, synthesized from polysaccharides derived from *Phlebopus portentosus*, displayed antioxidant, antibacterial, anti-cancer and anti-diabetic activities. These studies collectively confirm that polysaccharides can serve as effective reducing agents and stabilizers for silver nanoparticles, and it has been established that silver nanoparticles synthesized by polysaccharides possess substantial biological activity.

Therefore, this study aims to investigate the development and utilization of polysaccharide-mediated green synthesis of silver nanoparticles. Previous research conducted by our research group has revealed a high polysaccharide content in the fruits of *A. longiligulare*. The green synthesis of silver nanoparticles using polysaccharides offers a significant advantage by mitigating the harmful effects associated with traditional synthesis methods that rely on organic reagents. Currently, there is a lack of research focused on the green synthesis of silver nanoparticles utilizing the polysaccharides derived from *A. longiligulare* fruits. Therefore, the objective of this experiment is to synthesize nano-silver particles using polysaccharides extracted from these fruits. This study not only aims to enhancing the understanding of green synthesis methods for silver nanoparticles but also seeks to further develop and utilize the potential value of *A. longiligulare* fruits.

In this study, the polysaccharide component ALP-D was extracted from ALP and utilized as both a reducing agent and a stabilizing agent in the synthesis of AgNPs. The structure of the ALP-D component was characterized through ultraviolet-visible spectroscopy, monosaccharide component detection, molecular weight determination, Fourier transform infrared spectroscopy, Congo red assay and thermal stability analysis. The synthesis conditions for ALP(D)-AgNPs were optimized by SFE, resulting in the preparation of stable and uniform AgNPs. Subsequently, these nanoparticles were characterized using UV-Vis, FT-IR, TEM, XRD, and DLS techniques. Finally, the in vitro antioxidant activity of ALP(D)-AgNPs was evaluated using DPPH and ABTS free radical scavenging assays. The antibacterial activity of ALP (D)-AgNPs against E coli, S aureus, and B subtilis was assessed using the punching method. MIC and MBC of ALP(D)-AgNPs against E coli, S aureus and B subtilis were detected using 96-well plate method. The effects of MIC and MBC on the growth curves of E coli, S aureus and B subtilis were determined by OD. Additionally, the anticancer activity of ALP(D)-AgNPs on HepG2,Caco-2, C6, and MDA-MB-MB-231 cells was evaluated using the CCK-8 assay.

Materials and Methods

Materials and Reagents

The fruits of *A. longiligulare* were purchased from Baisha County, Hainan Province. After identification by Professor Tian Jianping, the voucher specimen (ALF202304) was preserved in the drying room of AB701 Chinese herbal medicine in the experimental building of Hainan Medical University, Haikou City, Hainan Province, China. Bacterial strains, including E coli, B subtilis, and S aureus were obtained from the Guangzhou Microbial Preservation Center. Silver

nitrate, sodium chloride, sodium hydroxide and anhydrous ethanol were purchased from Xilong Science Co., Ltd. Additionally, Congo red, ABTS and DPPH were sourced from Aladdin. Glucose and antihemorrhagic acid were procured from Tianjin Damao Chemical Reagent Factory. Potassium persulfate was supplied by Ron, while DEAE-52 was acquired from White Shark Reagent Co., Ltd. Sulfuric acid was purchased from Chengdu Cologne Chemicals Co., Ltd., and phenol was obtained from Xilong Chemical Co., Ltd. C6 and Caco-2 cells were purchased from ShangHai Saibaikang Biotechnology Co., Ltd. MDA-MB-231 and HepG2 cells were purchased from Wuhan Punosai Life Technology Co., Ltd.

Extraction, Separation and Purification of ALP

The extraction of ALP was conducted following the method described by Hu et al[18] with slight modification. The extraction process lasted for 1 h, was performed three times and occurred at a temperature of 100 °C. The liquid-to-solid ratios for the three extractions were 20:1, 15:1, and 10:1 (mL/g), respectively. The combined extract solution was concentrated to one-fifth of the original volume using a rotary evaporator to yield a concentrated solution. Anhydrous ethanol was then added to this concentrated solution at a ratio of 1:4. After mixing evenly, the solution was allowed to stand for 24 h at 4 °C, followed by filtration to obtain polysaccharide precipitation. The extracted polysaccharide was redissolved, and proteins were eliminated using the Sevag method. Finally, the polysaccharide solution was concentrated using a rotary evaporator, followed by dialysis (with a molecular weight cut-off of 3500 Da) and freeze-drying, resulting in the acquisition of crude polysaccharide.

A suitable quantity of crude polysaccharide was measured and dissolved in distilled water to create a 5 mg/mL crude polysaccharide solution. Following filtration, the sample was applied to a DEAE-52 cellulose column (2.5 × 40 cm) and eluted using a gradient of 0, 0.1, 0.2, 0.3, and 0.4 mol/L NaCl solutions. The elution rate was maintained at 2 mL/min, with each tube collecting 10 mL of eluent, resulting in a total of 80 tubes collected for each gradient. For detection, the phenol-sulfuric acid method was employed. Four elution components were identified: ALP-A, ALP-B, ALP-C, and ALP-D. Among these, ALP-D was the main component, and its eluent was then concentrated, dialyzed (with a molecular weight cut-off of 3500 Da) and lyophilized.

Characterization of ALP-D

Determination of Molecular Weight

The molecular weight of ALP-D was determined using high performance gel chromatography. The chromatographic column employed was a PL aquagel-OH Mixed-H, with detection performed using an evaporative light scattering detector. The sample concentration was established at 1 mg/mL, the mobile phase consisted of water, the flow rate was maintained at 1 mL/min, the column temperature was set to 30 °C, and the injection volume was 40 μL.

Monosaccharide Composition Analysis

The analysis of the monosaccharide composition of ALP-D was conducted following the method described by Gao et al[19] with minor modifications. In summary, ALP-D was hydrolyzed using 2 mol/L of trifluoroacetic acid, and the resulting hydrolyzed product was derivatized with 1-phenyl-3-methyl-5-pyrazolone (PMP). The analysis was then performed using HPLC with a Thermo Fisher UltiMate 3000 chromatograph, adhering to the same standard procedures applied to the twelve monosaccharides, which included hydrolysis followed by derivatization.

FT-IR and UV-Vis Analysis

ALP-D was mixed with potassium bromide (KBr) and compressed into pellets, after which the FT-IR spectrum was collected using the ShimadzuIRTracer 100 spectrometer in Japan, covering a range of 4000–400 cm^{-1}.

Additionally, ALP-D was dissolved in distilled water (1 mg/mL), and the ultraviolet spectrum was recorded in the range of 200–600 nm using a UV-Vis spectrophotometer (A590, AOE instrument, Shanghai, China).

Congo Red Test

The ALP-D Congo red detection method is based on the protocols established by Zhang Huihui et al[20] with slight modifications. Specifically, 2 mL of the ALP-D solution was mixed with 2 mL of the Congo red solution, followed by the

addition of varying volumes of 1 mol/L NaOH solution and distilled water, thereby adjusting the final concentration to a range of 0 to 0.5 mol/L. After allowing the mixture to react for 10 minutes in a dark environment, the maximum absorption wavelength of the resulting solution at different concentrations was measured using UV-Vis spectroscopy.

Thermal Stability Analysis

The thermogravimetric analyzer (PE-TGA4000, USA) was used to assess the thermal stability of ALP-D (4.39 mg). The nitrogen gas flow rate was maintained at 19.8 mL/min, while the temperature was incrementally increased at a rate of 10 °C per minute, rising from 30 °C to 800 °C.

Preparation of Silver Nanoparticles ALP(D)-AgNPs

Preparation of ALP-D, Silver Nitrate and ALP(D)-AgNPs Solution

Preparation of ALP-D Solution

Approximately 5 mg of ALP(D) was accurately weighed and transferred into a 50 mL beaker. Subsequently, 10 mL of distilled water was added to completely dissolve the compound, resulting in a 5 mg/mL ALP(D) solution. It is important to note that the ALP(D) solution is unstable and should be used promptly.

Preparation of Silver Nitrate Solution

A total of 850 mg of silver nitrate was accurately weighed and subsequently dissolved in distilled water. The resulting solution was then transferred to a 50 mL brown glass bottle to achieve a concentration of 100 mmol/L silver nitrate solution. As per the experimental requirements, ultrapure water was added to dilute the solution, resulting in a final concentration of 10 mmol/L silver nitrate.

Preparation of ALP(D)-AgNPs Solution

The preparation of the ALP(D)-AgNPs solution involved mixing 1 mL of the ALP(D) solution with 10 mL of silver nitrate solution in a 25 mL volumetric flask. Distilled water was then added to achieve a final volume of 25 mL. The reaction was conducted at a vibration frequency of 120 r/min, with a reaction time of 180 min at a temperature of 100 °C. After the reaction, the resulting ALP(D)-AgNPs solution was transferred to a cuvette, and its absorbance was measured at the maximum absorption peak within the range of 300 to 800 nm using a ultraviolet spectrophotometer, with water serving as the blank control.

Single Factor Experiment

Reaction Time

The volume ratio of the ALP-D solution to the silver nitrate solution was set at 1: 10. Then, the two solutions were mixed and transferred into a 25 mL volumetric flask. Distilled water was added to reach the designated scale line, and the reaction was conducted at 90 °C. Under these conditions, seven distinct nano-silver solutions were prepared corresponding to reaction times of 30, 60, 90, 120, 150, 180, and 240 min.

Reaction Temperature

The volume ratio of the ALP-D solution to the silver nitrate solution was maintained at 1:10. These solutions were then mixed and transferred into a 25 mL volumetric flask, to which distilled water was added up to the designated scale line. A total of five mixed solutions were prepared and allowed to react for 120 min at temperatures of 50, 60, 70, 80, and 90 °C, respectively.

Volume Ratio of ALP-D Solution to Silver Nitrate Solution

A volume of 1 mL of ALP-D solution (5 mg/L) was added to various volumes of silver nitrate solution (10 mmol/L), specifically 2, 6, 10, 12, and 14 mL, the resulting ALP(D) to silver nitrate ratios were 1:2, 1:6, 1:10, 1:12, and 1:14, respectively. The mixture was then diluted to 25 mL and subjected to a reaction at 90 °C for 120 min.

Characterization of ALP(D)-AgNPs

UV-Vis Spectrum

The synthesis of ALP(D)-AgNPs was confirmed using UV-Vis spectroscopy. The scanning wavelength range was established at 300 to 800 nm, and the UV-Vis spectrum of the ALP(D)-AgNPs was recorded within this range, utilizing distilled water as a blank control.

FT-IR Spectrum

ALP(D)-AgNPs were mixed with potassium bromide (KBr) powder and then compressed into flakes. The FT-IR spectrum was recorded on a Shimadzu IR Tracer 100 spectrometer in Japan, covering a range from 4000 to 400 cm^{-1}.

Particle Size and Potential Analysis

The zeta potential and particle size of the ALP(D)-AgNPs were measured using a DLS tester. The diluted ALP(D)-AgNPs solution was placed in a cuvette for analysis at 25 °C.

High Resolution Transmission Electron Microscopy (HRTEM)

The morphology of ALP(D)-AgNPs was examined using HRTEM. Initially, 10 μL of the ALP(D)-AgNPs solution was deposited onto a specialized copper mesh, allowing the water to evaporate naturally. The copper mesh was then mounted on the sampling table of the instrument and analyzed using transmission electron microscopy at an accelerating voltage of 200 kV.

X-Ray Diffraction

ALP(D)-AgNPs were characterized by XRD with a Bruker D8 Advance instrument from Germany. The analysis employed copper Kα radiation at 40 kV and 40 mA (λ = 1.54 A). The film sample was scanned from 10° to 80° at a scan rate of 0.3°/s.

Biological Activity of ALP(D)-AgNPs

Antioxidant Activity of ALP(D)-AgNPs in vitro

DPPH Free Radical Scavenging Activity

According to the established method in the literature,[21] 50 μL of a 0.1 mmol/L DPPH solution was introduced into 96-well plates, followed by the addition of 50 μL of ALP(D)-AgNPs at different concentrations. Anhydrous ethanol was used as the sample control group instead of DPPH, while deionized water served as the blank control group in place of the ALP(D)-AgNPs solution. Vitamin C was employed instead of ALP(D)-AgNPs. After thoroughly mixing the groups, the reaction was shielded from light for 30 min, and the absorbance was measured at 517 nm. The scavenging rate was calculated using the following formula: DPPH radical scavenging rate (%)=1-(A_1-A_2)/A_0×100. In this formula, A_0 represents the absorbance value of the blank control group, A_1 denotes the absorbance value of the sample determination group, and A_2 indicates the absorbance value of the sample control group.

ABTS Free Radical Scavenging Activity

Based on the methodology described in the literature with minor revisions,[22] ABTS was prepared by mixing 10 mL of a 7 mmol/L ABTS reserve solution with 100 mL of a 2.45 mmol/L $K_2S_2O_8$ solution, allowing the mixture to react in a refrigerator at 4 °C for 12 to 16 h. Prior to use, the ABTS was diluted with PBS to achieve an absorbance of 0.7 ± 0.02 at 734 nm, resulting in the ABTS working solution. A 50 μL aliquot of the ALP(D)-AgNPs solution, Vitamin C (as a positive control) or deionized water (as a blank) was placed in a 96-well plate. Distilled water served as the sample control group in place of the ABTS working solution, to which 50 μL of the ALP(D)-AgNPs solution was added and mixed thoroughly. After allowing the reaction to proceed in the dark for 6 min, the absorbance at 734 nm was measured using a microplate reader, and the ABTS free radical scavenging rate was calculated to assess the scavenging ability against ABTS free radicals. The formula for calculation is as follows: ABTS radical scavenging rate (%) = 1 - (A_1 - A_2) / A_0 × 100. In this formula, A_0 represents the absorbance value of the blank control group; A_1 denotes the absorbance value of the sample determination group; and A_2 indicates the absorbance value of the sample control group.

https://doi.org/10.2147/IJN.S501828

Antibacterial Activity of ALP(D)-AgNPs

Punching Method

Bacteria including E coli, S aureus and B subtilis were diluted to 10^6 CFU/mL using a sterile PBS solution, then 100 μL of the diluted cultures was evenly coated onto LB solid medium. A 10 mm puncher was employed to create wells into which 100 μL (1 mg/mL) of sterilized samples were introduced. The culture dish was then incubated at a constant temperature of 37 °C for 24 h. After the incubation period, the culture dish was removed, and the size of the inhibition zone was measured and recorded using a standard camera.

MIC and MBC of ALP(D)-AgNPs

Bacterial strains including *E. coli,* S aureus, and B subtilis were diluted to 10^6 CFU/mL using LB liquid medium for subsequent use. The sample solution was further diluted to a concentration of 0.5 mg/mL in LB liquid medium. Subsequently, 100 μL of LB liquid medium was added to wells two through twelve of a 96-well plate, while 200 μL of the 1 mg/mL sample-medium mixture was added to the first well. Next, 100 μL of the sample-medium mixture was transferred to the second well, followed by an additional 100 μL to the third well. This dilution process was continued, resulting in a twofold dilution of the sample solution. Finally, 100 μL of the sample-medium mixture was withdrawn from the twelfth well and discarded. The sample solution was then replaced with PBS solution, and the previous steps were repeated to serve as the control group. A 100 μL diluted bacterial solution was added to each well of the 96-well plate, resulting in an initial sample concentration of 0.5 mg/mL. The plates were incubated at a constant temperature of 37 °C for 24 h, after which the MIC values were photographed and recorded. Subsequently, the first turbid well and the first two clear wells were selected for coating and placed in a constant temperature incubator at 37 °C for 18 h. The number of colonies was then counted and recorded, resulting in a colony count of 0, which indicated the MBC value.

Growth Curves of E coli, B subtilis and S aureus

During the logarithmic phase, the concentrations of the three test bacteria were diluted to 1×10^6 CFU/mL. ALP(D)-AgNPs were then added to the solution at their respective MIC and MBC values, with saline serving as a control. The mixed solution was then cultured in a shaker at 37 °C (150 r/min). The OD value at 600 nm was measured at regular intervals over a 0 to 24 h using a UV-Vis spectrophotometer, allowing for the generation of a growth curve.

Anticancer Activity of ALP(D)-AgNPs

Cell Culture

Tumor cells, including HepG-2, C6, and MDA-MB-231, were maintained in a complete medium consisting of DMEM supplemented with 10% fetal bovine serum at 37 °C. Caco-2 human colorectal adenocarcinoma cells were cultured in a complete medium composed of MEM with 10% fetal bovine serum and were kept in a humidified CO_2 incubator. The cells were harvested by trypsinization and subsequently seeded into culture plates or Petri dishes as per experimental requirements.

Cytotoxicity Assay

The cytotoxicity of ALP(D)-AgNPs was assessed using the CCK8 assay. HepG-2, C6, Caco-2, and MDA-MB-231 cells (1×10^4 cells/well) were plated in 96-well plates and cultured for 24 h to allow for adhesion and growth. Following this incubation period, the medium was removed, and the cells were exposed to various concentrations of ALP(D)-AgNPs for an additional 24 h. The concentration range of ALP(D)-AgNPs tested was 0 to 64 μg/mL.

Statistical Analysis

Statistical analysis was conducted using GraphPad Prism version 9.5.1 software. All quantitative data are expressed as mean ± standard deviation ($\bar{x} \pm s$). Additionally, Origin 9.0 software (OriginLab company, United States) was utilized for graphic analysis.

Results

Extraction, Separation and Purification of ALP

The process of extraction and separation of ALP is illustrated in Figure 1A. The crude polysaccharide was separated by DEAE-52 column chromatography. As depicted in Figure 1B, four elution peaks were obtained: ALP-A, ALP-B, ALP-C, and ALP-D, with respective yields of were 0.24%, 1.74%, 2.87%, and 9.45% for each component.

Characterization of ALP-D

Determination of Molecular Weight

As shown in Figure 2A, the HPGPC spectrum of the purified ALP-D exhibited a single symmetrical peak with a retention time of 20 min. The number average molecular weight (Mn) of ALP-D was determined to be 22,448 Da, while the weight average molecular weight (Mw) was 45,984 Da, and the peak molecular weight (Mp) was 25,402 Da. The calculated polydispersity index (PDI) obtained by dividing Mw by Mn, was found to be 2.04. This result indicates that the molecular weight distribution of the synthesized ALP-D is broad and irregular. Therefore, it is speculated that ALP-D is not a homogeneous polysaccharide and may contain some low molecular weight components.

Monosaccharide Composition Analysis

As shown in Figures 2B and C, ALP-D primarily consists of nine monosaccharides: mannose, rhamnose, glucuronic acid, galacturonic acid, glucose, galactose, xylose, arabinose, and fucose. The relative contents of these monosaccharides are 2.34%, 9.47%, 3.29%, 57.17%, 2.37%, 8.46%, 6.45%, 9.78%, and 0.67%, respectively. Thus, ALP-D is classified as an acidic polysaccharide, mainly composed of galacturonic acid.

FT-IR and UV-Vis Spectra

The FT-IR spectrum of ALP-D, presented in the range of 4000–400 cm^{-1}, exhibits the typical absorption characteristics of polysaccharides, as shown in Figure 2D.[23] The prominent and broad peak around 3417 cm^{-1} corresponds to O-H stretching vibrations, while the peak at 2937 cm^{-1} represents C-H stretching bands. The absorption band observed at 1610 cm^{-1} is associated with carbonyl (C=O) stretching vibrations, and the peaks at 1415 cm^{-1} and 1330 cm^{-1} are attributed to C-H bending vibrations.[24] Additionally, the absorption peaks at 1095 cm^{-1} and 1022 cm^{-1} correspond to the

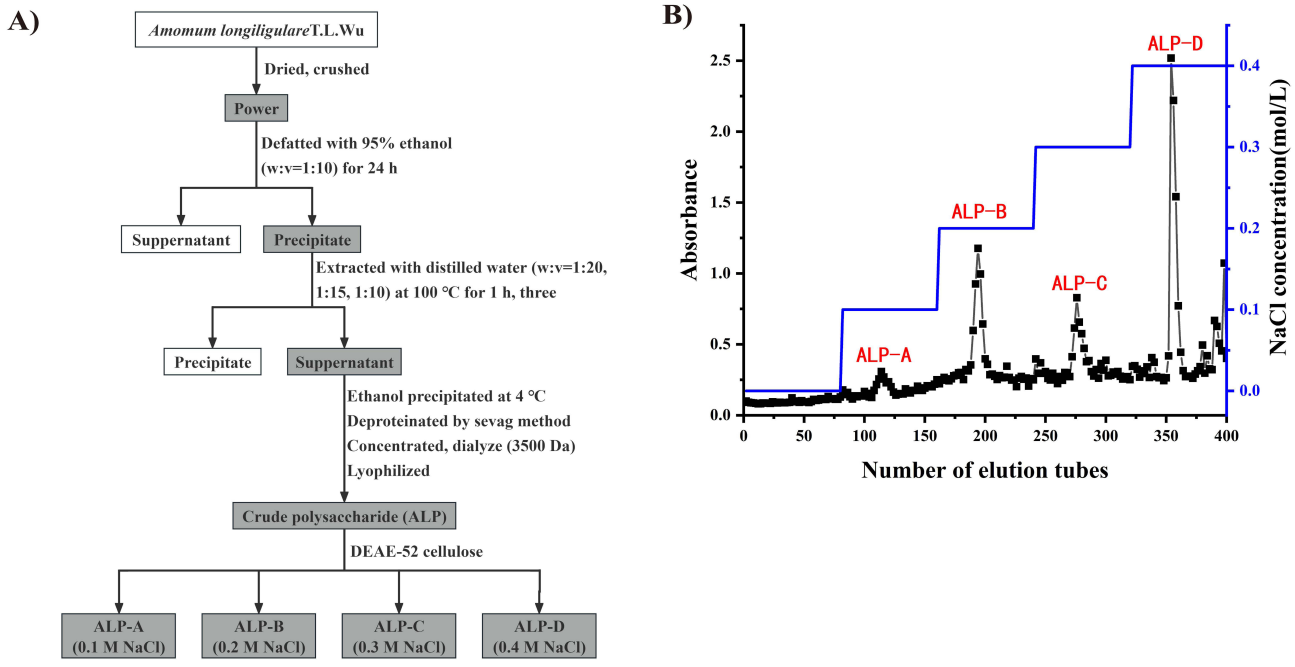

Figure 1 Extraction and purification of ALP. (**A**) Preparation flow chart of ALP. (**B**) Elution curve of ALP on DEAE-52 cellulose column.

https://doi.org/10.2147/IJN.S501828

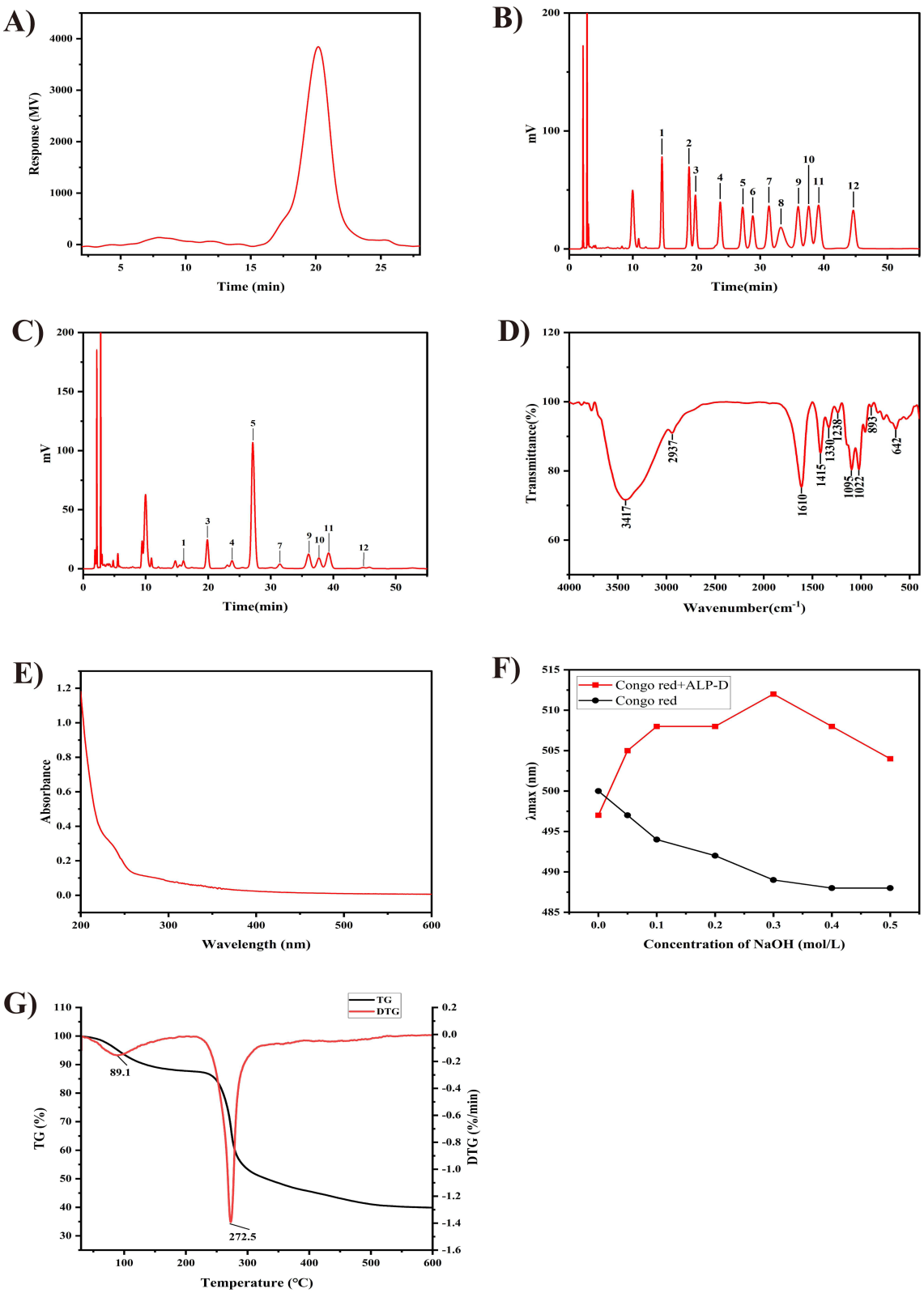

Figure 2 Characterization of ALP-D. (**A**) Molecular weight analysis of ALP-D. (**B**) Monosaccharide standard (1.Mannose, 2. Ribose, 3. Rhamnose, 4. Glucuronic acid, 5. D-Galacturonic acid, 6. N-acetylglucosamine, 7. Glucose, 8. N-acetylgalactosamine, 9. Galactose, 10. Xylose, 11. Arabinose, 12. Fucose). (**C**) Monosaccharide composition of ALP-D. (**D**) FT-IR analysis of ALP-D. (**E**) UV-Vis of ALP-D. (**F**) Congo red analysis of ALP-D. (**G**) Thermal stability analysis of ALP-D.

stretching vibrations of pyranose.[25] Moreover, the faint peak around 893 cm^{-1} confirms the presence of α-configuration glycosidic bonds.[26]

The UV-Vis spectrum of ALP-D, shown in Figure 2E, reveals no significant absorption peaks at 260 nm and 280 nm, suggesting that ALP-D is essentially free of nucleic acids and proteins.[27]

Congo Red Test

As the concentration of NaOH increased, the structure of the Congo red complex was disrupted, resulting in a decrease in the maximum absorption wavelength of the solution.[28] Figure 2F illustrates that the maximum absorption wavelength of the solution gradually increases as the NaOH concentration rises from 0 to 0.3 mol/L. Conversely, when the NaOH concentration exceeds 0.3 mol/L, the maximum absorption wavelength starts to decrease gradually. These findings suggest that ALP-D possesses a triple helix structure.[29]

Thermal Stability Analysis

The TG curve presented in Figure 2G illustrates that the thermal weight loss process of ALP-D occurs in three distinct stages. The initial stage, which takes place between 32 and 160 °C, is characterized by a weight loss rate of 11.18%. The second stage, occurring between 160 and 490 °C, exhibits a weight loss rate of 47.29%, indicating that the polysaccharide undergoes a vigorous reaction within this temperature range. In the third stage, from 490 to 600 °C, the weight change of the polysaccharide becomes more gradual, ultimately reaching a state of thermal stability.

Synthesis of ALP(D)-AgNPs

In this study, ALP(D)-AgNPs were synthesized using a green method, with ALP(D) serving as both the stabilizer and reducing agent. Figure 3A illustrates the effect of reaction time on the synthesis of ALP(D)-AgNPs. The formation of silver nanoparticles was assessed using UV-Vis absorption spectroscopy to identify a peak around 420 nm. The results

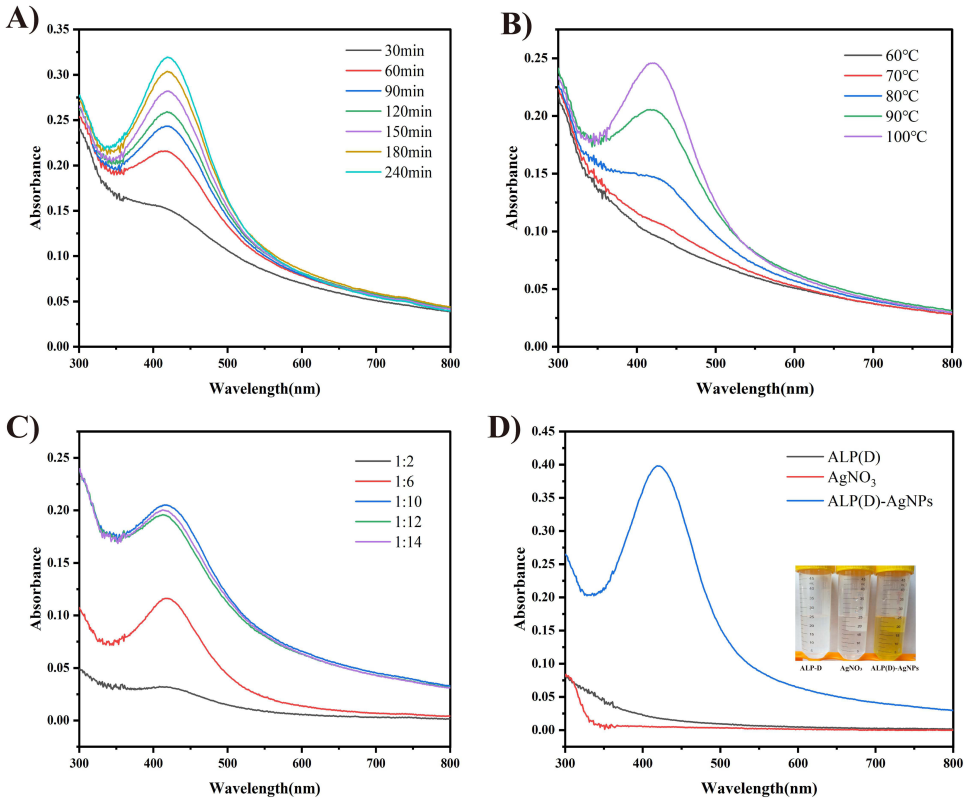

Figure 3 UV-Vis of silver nitrate and ALP-D mixed solution under different conditions. (**A**) UV-Vis spectra at different times. (**B**) UV-Vis spectra at different temperatures. (**C**) UV-Vis of different volume ratios of ALP-D to silver nitrate. (**D**) UV-Vis of ALP-D, AgNO3 and ALP(D)-AgNPs.

https://doi.org/10.2147/IJN.S501828

indicated a distinct maximum absorption peak at this wavelength, with the absorbance value increasing progressively as the reaction time extended, suggesting a corresponding rise in nanoparticle concentration. During the time interval from 30 to 180 min, the absorbance of ALP(D)-AgNPs exhibited significant changes, peaking at 240 min. However, from 180 to 240 min, the absorbance of the nano-silver complex showed minimal variation. Thus, we selected 180 min as the optimal reaction time.

Figure 3B illustrates the effect of reaction temperature on the synthesis of ALP(D)-AgNPs. Notably, no maximum absorption peaks are observed in the UV-Vis spectrum at 60 and 70 °C, indicating that the nano-silver complex is not produced at these temperatures. In contrast, maximum absorption peaks appear in the UV-Vis spectrum at 80, 90, and 100 °C, with absorbance values increasing progressively as the reaction temperature rises. This trend demonstrates the dependence of ALP(D)-AgNPs synthesis on reaction temperature, leading us to select 100 °C as the optimal reaction temperature.

Figure 3C depicts the impact of the volume ratio of ALP(D) to silver nitrate on the synthesis of ALP(D)-AgNPs. As the volume ratio of ALP(D) to silver nitrate increases from 1:2 to 1:10, the absorbance value of ALP(D)-AgNPs gradually rises. However, from a ratio of 1:10 to 1:14, the absorbance value decreases, potentially due to the formation of larger particles or clusters of unformed AgNPs.[30] Therefore, a volume ratio of ALP(D) to silver nitrate of 1:10 is selected as the optimal reaction condition.

Based on the findings from the single-factor experiments, the optimal conditions for synthesizing ALP(D)-AgNPs are established as follows: a volume ratio of ALP(D) to silver nitrate of 1:10, a reaction time of 180 minutes, and a reaction temperature of 100 °C.

Characterization of ALP(D)-AgNPs

UV-Vis Spectrum

The synthesis of ALP(D)-AgNPs was conducted under optimal conditions, and their spectra were analyzed using UV-Vis spectroscopy over the range of 300 to 800 nm. As illustrated in Figure 3D, the results indicated that ALP(D)-AgNPs exhibited an absorption peak at 420 nm, whereas neither ALP(D) nor silver nitrate displayed any absorption peaks. Furthermore, the UV-Vis spectrum of ALP(D)-AgNPs revealed a singular peak at 420 nm without any additional absorption peaks, thereby confirming the successful formation of ALP(D)-AgNPs.[15]

FT-IR Spectrum

Figure 4A shows that the FT-IR spectra of ALP-D and ALP(D)-AgNPs exhibit similar characteristic peaks, indicating their fundamental similarity. However, most characteristic peaks associated with the functional groups of ALP(D)-AgNPs exhibit a red shift and a decrease in peak intensity, which may result from the interaction between AgNPs and the functional groups in ALP-D.[31] These findings indicate that the functional groups in ALP-D are essential for the synthesis of silver nanoparticles.

Analysis of Particle Size and Potential

As shown in Figure 4C, the results of dynamic light scattering (DLS) indicate that the particle size of ALP(D)-AgNPs in aqueous suspension is 148 nm. Additionally, Figure 4B illustrates that the zeta potential is −33.25 mV. The absolute value of the zeta potential of ALP(D)-AgNPs exceeds 20 mV, indicating that the stability of ALP(D)-AgNPs is favorable.[32]

High Resolution Transmission Electron Microscopy (HRTEM)

The shape, size and distribution of the synthesized ALP(D)-AgNPs were verified by HRTEM. As illustrated in Figure 5, the transmission electron microscope image reveals that the particles are spherical, well-dispersed, and exhibit no obvious aggregation. The histogram of particle size distribution indicates that the size of the silver nanoparticles ranges from 12 to 44 nm, with an average particle size of 29.64 nm.

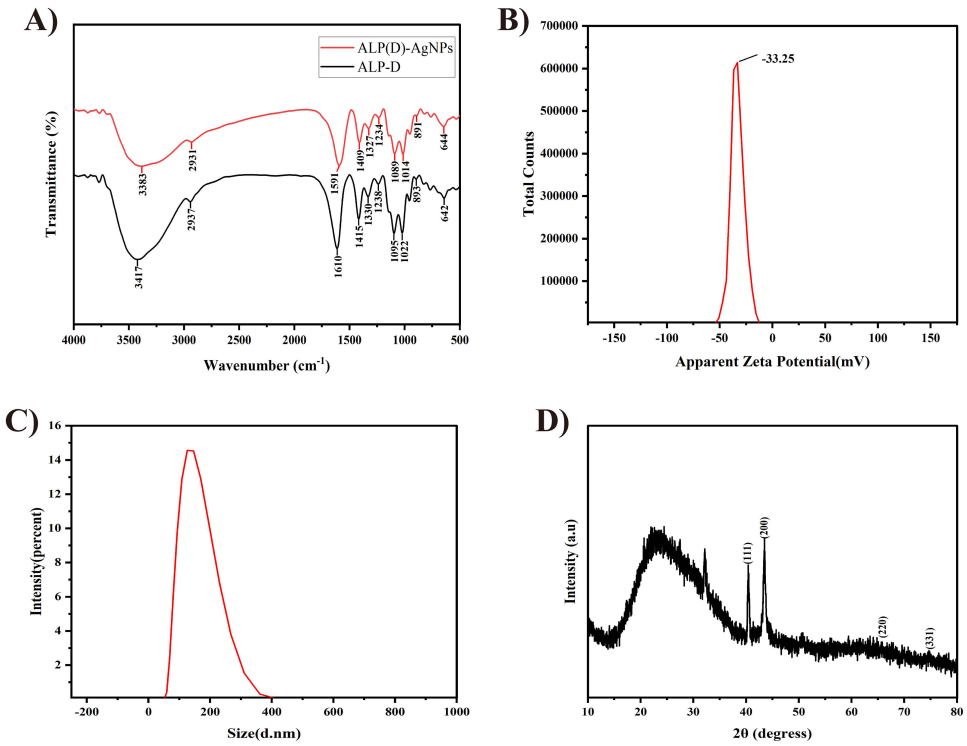

Figure 4 Characterization of ALP(D)-AgNPs. (**A**) FT-IR of ALP(D)-AgNPs. (**B**) Zeta potential of ALP(D) -AgNPs. (**C**) The water dynamic particle size of ALP(D)-AgNPs. (**D**) X-ray diffraction analysis of ALP(D)-AgNPs.

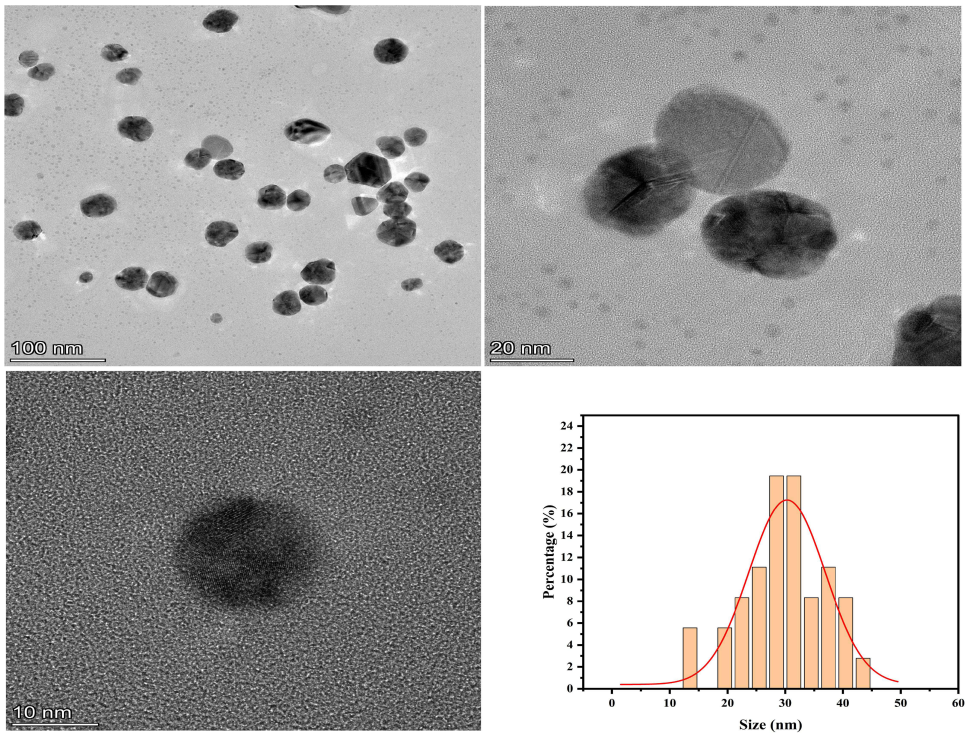

Figure 5 HRTEM image and particle size distribution of ALP(D)-AgNPs.

https://doi.org/10.2147/IJN.S501828

X-Ray Diffraction (XRD)

As shown in Figure 4D, XRD analysis reveals that ALP(D)-AgNPs exhibit four distinct diffraction peaks at 40.04°, 43.50°, 65.83°, and 74.68°, corresponding to the crystal planes of 111, 200, 220, and 331, respectively. These values indicate that ALP(D)-AgNPs possess a face-centered cubic crystal structure.[33]

Biological Activity

Antioxidant Activity of ALP(D)-AgNPs in vitro

DPPH Free Radical Scavenging Activity

Figure 6A presents the DPPH free radical scavenging rates for both ALP(D)-AgNPs and ALP-D. The scavenging rates of ALP(D)-AgNPs were recorded at 36.61%, 37.94%, 48.73%, 55.51%, 71.20%, and 76.20% for concentrations of 0.05, 0.1, 0.2, 0.4, 0.8, and 1 mg/mL, respectively. These data indicate that the scavenging activity of ALP(D)-AgNPs is concentration-dependent, demonstrating an increase in activity with rising concentration, culminating in a maximum rate of 76.20%. The half-scavenging concentration (half-inhibitory concentration) for ALP(D)-AgNPs was determined to be 0.21 mg/mL.

ABTS Free Radical Scavenging Activity

Figure 6B presents the results of the ABTS radical scavenging activity for both ALP(D)-AgNPs and ALP-D. The ABTS radical scavenging rates for ALP(D)-AgNPs were recorded at 16.18%, 17.62%, 21.70%, 26.54%, 40.93%, and 47.83% at concentrations of 0.05, 0.1, 0.2, 0.4, 0.8, and 1 mg/mL, respectively. This indicates that the ABTS radical scavenging activity of ALP(D)-AgNPs is concentration-dependent, increasing with higher concentrations, and ultimately reaching a maximum scavenging rate of 47.83%. In contrast, the ABTS free radical scavenging activity of ALP-D at the same concentrations (0.05, 0.1, 0.2, 0.4, 0.8, and 1 mg/mL) was 0.99%, 6.90%, 7.67%, 13.03%, 16.87%, and 17.31%, respectively, with a maximum scavenging rate of 17.31%. These results demonstrate that the synthesized silver nanoparticles [ALP(D)-AgNPs] exhibit a significantly stronger ABTS free radical scavenging rate compared to ALP-D.

Antibacterial Activity of ALP(D)-AgNPs

Punching Method

In this study, S aureus, B subtilis and E coli were selected as representatives of Gram-positive and Gram-negative bacteria. The results obtained from the punching method are presented in Figure 7A-C and Table 1. S aureus exhibited the highest resistance to ALP(D)-AgNPs at a concentration of 1 mg/mL, resulting in the smallest inhibition zone diameter of 8.33 ± 0.57 mm. In contrast, B subtilis demonstrated the greatest sensitivity at the same concentration, with an inhibition zone diameter of 10.33 ± 0.57 mm. The control group of all three bacteria exhibited robust growth, indicating that the observed antibacterial activity can be attributed to the nanoparticles.

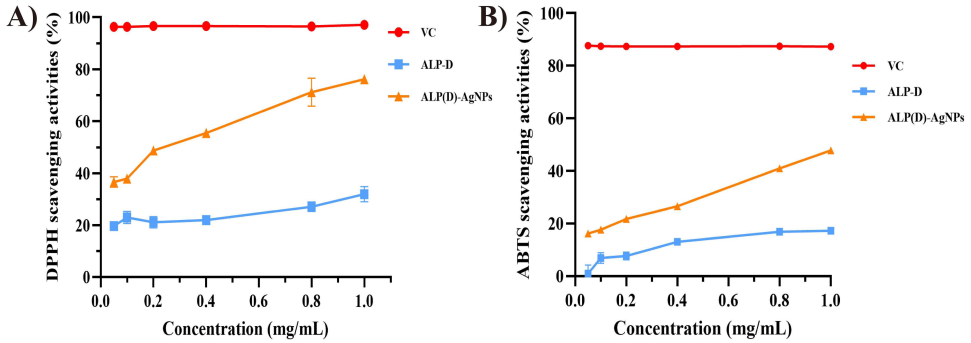

Figure 6 Antioxidant activity of ALP(D)-AgNPs in vitro. (**A**) DPPH radical scavenging activity of ALP(D)-AgNPs. (**B**) ABTS radical scavenging activity of ALP(D)-AgNPs.

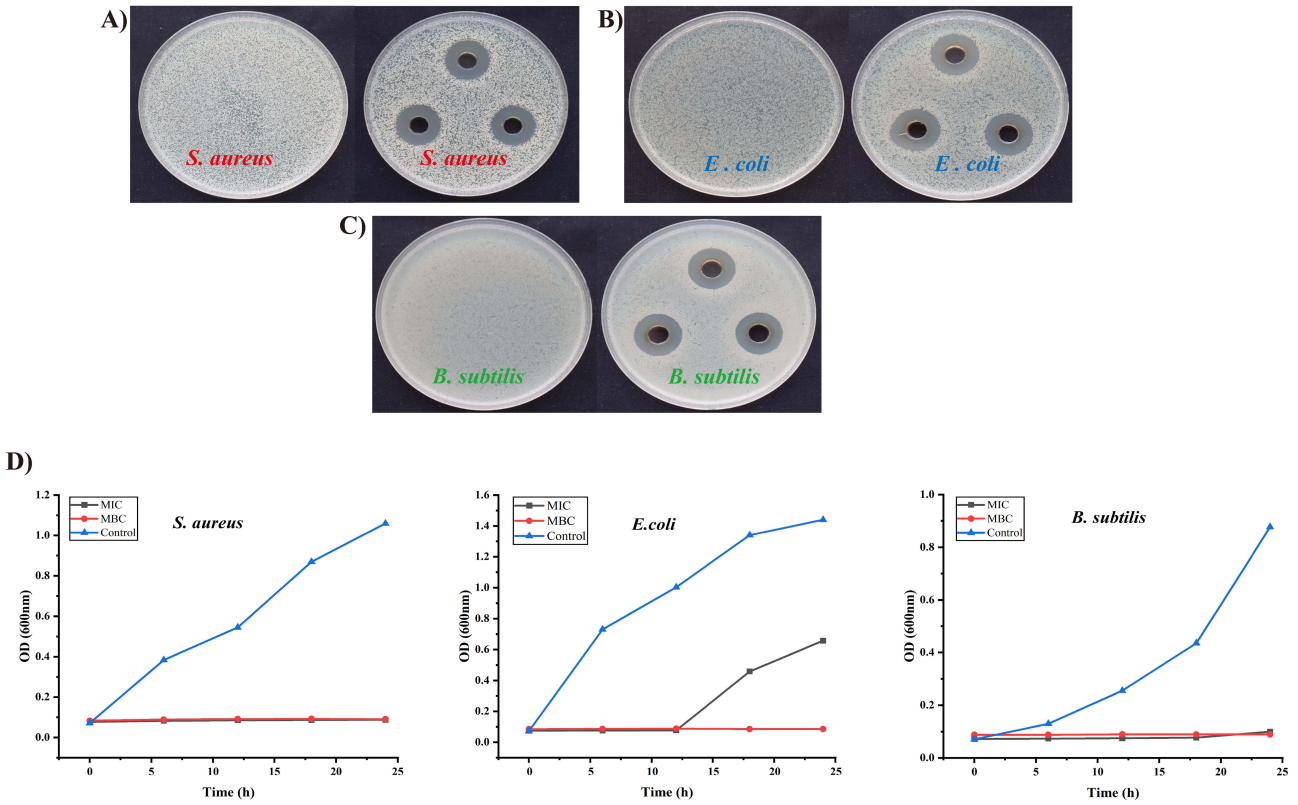

Figure 7 Antibacterial activity of ALP-AgNPs. (**A**) The inhibition zone of S aureus. (**B**) The inhibition zone of E coli. (**C**) The inhibition zone of B subtilis. (**D**) The growth curves of S aureus, E coli and B subtilis at 24 h were determined in ALP(D)-AgNPs with MIC and MBC concentrations and saline.

MIC and MBC of ALP(D)-AgNPs

As indicated in Table 2, the MIC values of ALP(D)-AgNPs against E coli and B subtilis were 31.25 μg/mL, while the MIC value for S aureus was 62.5 μg/mL. The MBC values of ALP(D)-AgNPs for E coli, S aureus, and B subtilis were all 125 μg/mL.

Table 1 Inhibition Zone of ALP(D)-AgNPs

Sample	Diameter of inhibition zone (mm)
S aureus (ATCC29213)	8.33±0.57
E coli (ATCC25922)	10.00±0
B subtilis (ATCC6633)	10.33±0.57

Table 2 MIC and MBC of ALP(D)-AgNPs for Different Bacteria

Sample	MIC (μg/mL)	MBC (μg/mL)
S aureus (ATCC29213)	62.5	125
E coli (ATCC25922)	31.25	125
B subtilis (ATCC6633)	31.25	125

https://doi.org/10.2147/IJN.S501828

Growth Curves of E coli, B subtilis and S aureus

The growth curve presented in Figure 7D illustrates that the number of bacteria treated with ALP(D)-AgNPs at the MIC was reduced, indicating an inhibition of growth. Notably, the bacteria count of E coli showed a significant increase at 16 h and 24 h, indicating that the antibacterial efficacy of ALP(D)-AgNPs against E coli is inferior to that observed for S aureus and B subtilis. However, when the concentration of ALP(D)-AgNPs was increased to MBC, the OD value at 600 nm for the three bacterial cultures exhibited minimal increase. These results suggest that ALP(D)-AgNPs possess broad-spectrum antibacterial properties.

Anticancer Activity of ALP(D)-AgNPs

The anticancer activity of ALP(D)-AgNPs on MDA-MB-231, HepG2, Caco-2 and C6 cell lines was assessed using the CCK-8 assay. As illustrated in Figure 8, the synthesized ALP(D)-AgNPs exhibited dose-dependent cytotoxicity towards these cancer cell lines, although the sensitivity varied among them. Table 3 presented the IC50 values of ALP(D)-AgNPs for the MDA-MB-231, HepG2, Caco-2, and C6 cancer cell lines, which were found to be 14.72 ± 0.23, 8.19 ± 0.65, 22.73 ± 3.01, and 15.77 ± 2.91 μg/mL, respectively. These results indicate that the synthesized ALP(D)-AgNPs exhibit significant toxicity towards all cancer cell lines at their half-inhibitory concentrations.

This study highlights the effectiveness of ALP(D)-AgNPs in inducing cell death in MDA-MB-231, HepG2, Caco-2, and C6 cells, suggesting their potential application in the development of anticancer drugs.

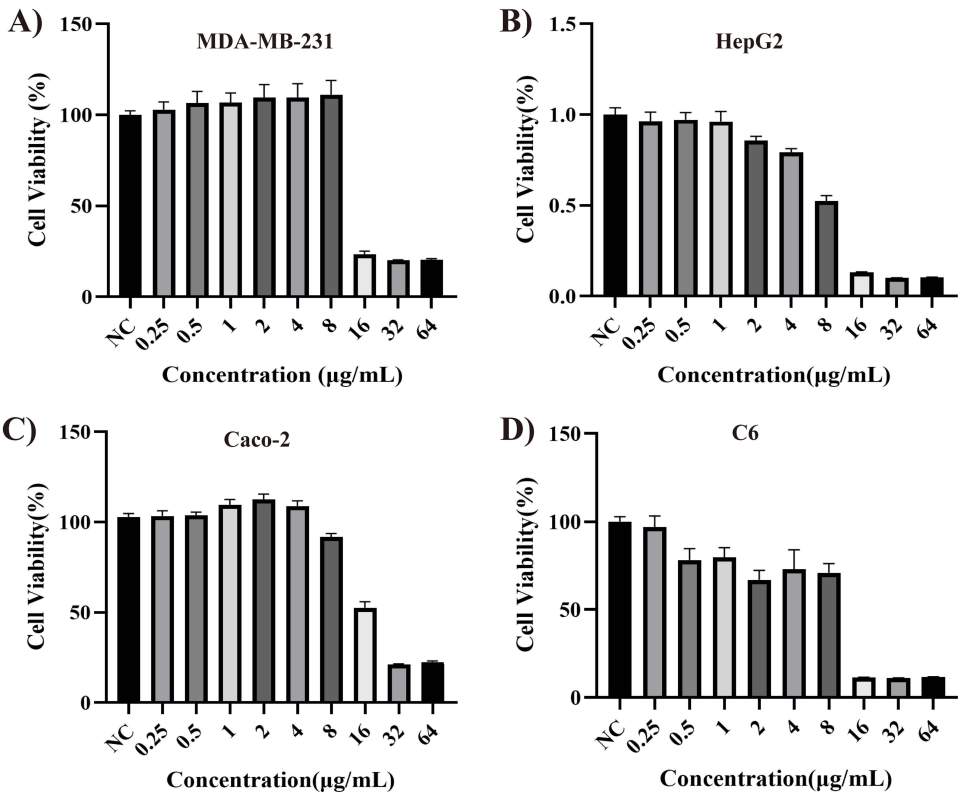

Figure 8 Anti-cancer effects of ALP(D)-AgNPs. (**A**) The anticancer effect of ALP(D)-AgNPs on MDA-MB-231 cells. (**B**) The anticancer effect of ALP(D)-AgNPs on HepG2 cells. (**C**) The anticancer effect of ALP(D)-AgNPs on Caco-2 cells. (**D**) The anticancer effect of ALP(D)-AgNPs on C6 cells.

Table 3 Anti-Cancer Effect of ALP(D)-AgNPs

Sample	IC_{50} (μg/mL)			
	MDA-MB-231	HepG2	Caco-2	C_6
ALP(D)-AgNPs	14.72±0.23	8.19±0.65	22.73±3.01	15.77±2.91

Discussion

In this study, ALP-D was utilized as a reducing agent and stabilizer for the synthesis of nano-silver, resulting in the successful production of nano-silver particles [ALP(D)-AgNPs]. The structure of ALP(D)-AgNPs was characterized by FT-IR, UV-vis, TEM and XRD techniques. The green-synthesized ALP(D)-AgNPs exhibited structural characteristics similar to those reported in previous studies. For example, UV-vis analysis revealed that the maximum absorption wavelength of the synthesized nano-silver particles was 419 nm, which falls within the expected range for the nano-silver particles. Additionally, the synthesized nano-silver solution exhibited a yellow color, consistent with findings from prior research.[31] Furthermore, investigations into the biological activity demonstrated that ALP(D)-AgNPs possessed notable antibacterial and anticancer properties.

In contrast to many studies focusing on the synthesis of AgNPs using plant crude polysaccharides alone, the use of purified and separated polysaccharides (ALP-D) represents an innovative approach. This method specifically explore the role of polysaccharides in the synthesis of nano-silver, effectively eliminating the influence of pigments and small molecular impurities. Research has demonstrated that polysaccharides with a triple helix structure can promote the effective dispersion of silver nanoparticles in water, serving as a dispersing agent during the synthesis process of silver nanoparticles and preventing the aggregation of the nanoparticles.[34] This experimental study confirmed that ALP-D possesses a triple helix structure. It was found by HRTEM that ALP(D)-AgNPs exhibited excellent dispersibility. Notably, the synthesized nano-silver particles [ALP(D)-AgNPs] remained suspended without precipitation for two weeks, indicating not only good dispersibility but also significant stability.

This study found that ALP(D)-AgNPs exhibited excellent antibacterial activity against both Gram-negative bacteria (E coli) and Gram-positive bacteria (S aureus and B subtilis). The MBC values of ALP(D)-AgNPs against E coli, S aureus and B subtilis were determined to be 125 μg/mL. Previous reports indicates that a decrease in the particle size of AgNPs enhances their efficacy in killing both Gram-negative and Gram-positive bacteria.[35] This enhancement is attributed to the ability of smaller AgNPs to penetrate bacterial cell membrane more readily, as their surface area is considerably larger than that of larger AgNPs, thereby increasing the likelihood of interaction with bacterial cells.[36] For instance, Talib et al found that silver nanoparticles synthesized using methanol extract were smaller than those synthesized from water extract, with Met-AgNPs demonstrating the highest antibacterial activity against *Pseudomonas aeruginosa*. This observation may be linked to the size of the particles, as Met-AgNPs are smaller than Aq-AgNPs.[37] Additionally, Xiong et al reported that silver nanoparticles of varying particle sizes (5 nm, 50 nm, 100 nm) exhibit different antibacterial properties, with 5 nm nanoparticles showing the highest antibacterial activity.[38] Agnihotri et al prepared AgNPs ranging from 5 to 100 nm and found that AgNPs smaller than 10 nm had a more pronounced bactericidal effect on E coli compared with larger AgNPs.[39] In this study, the particle size of the synthesized nano-silver ALP(D)-AgNPs ranged from 12 to 44 nm. The synthesized nano-silver particles exhibited a small size, which contributed to their effective antibacterial activity against bacteria. Consequently, it is crucial in this study to utilize ALP-D for the reduction, dispersion, and stabilization of AgNPs, as these factors may directly influence the functionality of silver nanoparticles. However, the antibacterial mechanism of ALP(D)-AgNPs remains unclear. Research indicates that the penetration of AgNPs into the inner membrane of cells can lead to the inactivation of respiratory chain dehydrogenase, thereby inhibiting cellular respiration and growth.[40] Additionally, it has been reported that the antimicrobial activity of AgNPs in aqueous media is associated with their surface oxidation and the release of Ag ions.[41]

https://doi.org/10.2147/IJN.S501828

The IC50 values ALP(D)-AgNPs against the MDA-MB-231, HepG2, Caco-2 and C6 cancer cell lines were 14.72 ± 0.23, 8.19 ± 0.65, 22.73 ± 3.01, and 15.77 ± 2.91 μg/mL, respectively. These IC50 values indicated that ALP(D)-AgNPs exhibit significant and broad-spectrum anticancer activity. Studies demonstrates that silver nanoparticles can induce apoptosis, cause DNA fragmentation, and inhibit cell proliferation in cancer cells.[42] The enhanced cytotoxicity of ALP (D)-AgNPs in the MDA-MB-231, C6, HepG2 and Caco-2 cell lines may be attributed to their increased cellular uptake and stability. Research has shown that AgNPs are not significantly affected by β-glycoprotein efflux, allowing them to easily penetrate cancer cells due to their smaller size and larger surface area.[43] Previous studies have also indicated that AgNPs synthesized using polysaccharides possess considerable anticancer potential. For example: Devasvaran et al employed crude polysaccharide extracted from *Clinacanthus nutans* using an alkaline method to synthesize AgNPs via microwave-assisted green synthesis, resulting in an average particle diameter of 7.48 ± 2.88 nm. The IC50 values of ALK-AgNPs for MCF-7 and HT-29 cells were recorded at 5.08 ± 0.97 μg/mL and 5.46 ± 0.16 μg/mL, respectively.[44] Additionally, Bidhayak et al extracted polysaccharide from *Acalypha australis* to serve as a reducing agent and stabilizer in the preparation of polysaccharide nano-silver particle complexes with particle sizes ranging from 7.25 nm to 92.51 nm. The presence of silver in PS-AgNPs was confirmed through energy dispersive X-ray (EDX) analysis, demonstrating that PS-AgNPs exhibit certain anticancer activity.[45] *Platinum spirulina* polysaccharide (PSP) has been demonstrated to synthesize silver nanoparticles (AgNPs) through a green manner, and its potential role in cancer treatment has been established. Specifically, the AgNPs derived from PSP exhibit superior anticancer activity against liver cancer cell lines, with an IC50 value of 24.5 μg/mL.[46] Studies indicate that the cytotoxicity of silver nanoparticles is influenced by factors such as particle size and concentration; larger particles generally exhibit lower toxicity compared to smaller ones, while higher concentrations are more likely to induce cellular damage.[37] In this experiment, the particle size of the nano-silver synthesized via green synthesis was measured at 29.64 nm. It was observed that ALP(D)-AgNPs demonstrated significant antitumor activity against four different cancer cell lines. In line with previous research findings, smaller particle sizes of nano-silver correlate with enhanced antitumor efficacy.

Conclusion

In this study, ALP-D was extracted and isolated from the fruits of *A. longiligulare* using a water extraction method followed by alcohol precipitation. Several structural features of ALP-D were identified through various characterization techniques. Following this, ALP(D)-AgNPs were successfully synthesized via a green chemical method, with ALP-D serving as both a stabilizing and reducing agent. The size, stability, morphology, and structure of ALP(D)-AgNPs were characterized by different methods. Biological activity assays demonstrated that ALP(D)-AgNPs exhibited certain antioxidant capacity and antibacterial activity. Additionally, ALP(D)-AgNPs displayed anticancer activity against MDA-MB-231, HepG2, Caco-2 and C6 cancer cell lines. Notably, the preparation of ALP(D)-AgNPs was achieved through a method characterized by low energy consumption and minimal toxic side effects on the environment. This study provides a novel approach to the preparation of nano-silver materials and proposes an innovative pathway for the development and utilization of the fruits of *Amomum longiligulare*. However, it is important to note that this study only explored the antibacterial and anticancer activities of ALP(D)-AgNPs at a preliminary level. While notable antibacterial properties were observed, the mechanisms underlying their anticancer and antibacterial effects remain unclear. Therefore, we plan to conduct further investigations into the antibacterial and anticancer mechanisms of ALP(D)-AgNPs in the future.

Abbreviations

ALP, *Amomum longiligulare* fruit polysaccharide; CCK-8, Cell Counting Kit-8; FT-IR, Fourier Transform Infrared Spectrometer; UV-Vis, Ultraviolet and visible spectrophotometry; MIC, Minimum inhibitory concentration; MBC, Minimum bactericidal concentration; HepG2, human hepatocellular carcinomas; C6, rat C6 glioma cells; Caco-2, human colorectal adenocarcinoma; MDA-MB-231, human breast cancer cells; S Aureus, Staphylococcus aureus; E coli, Escherichia coli; B Subtilis, Bacillus subtilis; SFE, Single factor experiment; XRD, X-ray diffraction; ALP-D, ALP (D); TEM, transmission electron microscopy; AgNPs, Silver nanoparticles; DLS, dynamic light scattering; IC50, Half maximal inhibitory concentration.

Acknowledgments

This work was supported by Hainan Provincial Natural Science Foundation of China (821RC743), National Natural Science Foundation of China (82460779), and the Hainan Province Clinical Medical Center (QWYH202175).

Disclosure

The authors report no conflicts of interest in this work.

References

1. National Pharmacopoeia Commission. Pharmacopoeia of the People ‘s Republic of China (Volume 1). *China Pharma Sci Technol Press*. 2020;1:264–265.
2. Fu YJ, Jiang XL, Zhang S, et al. Optimization of extraction process of Amomum longiligulare T. L. Wu polysaccharides by response surface methodology. *J Hainan Medl Univ*. 2021;27(06):467–471.
3. Wei Z, Ruan XM, Dai TT, et al. Structure characterization and antioxidant activity of polysaccharides from Amomum villosum extracted with alkaline solution. *Sci Technol Food Ind*. 2021;42(24):87–93.
4. Wang L, Xie J, Huang T, et al. Characterization of silver nanoparticles biosynthesized using crude polysaccharides of Psidium guajava L. leaf and their bioactivities. *Mater Lett*. 2017;208:126–129. doi:10.1016/j.matlet.2017.05.014
5. El-Rafie HM, El-Rafie MH, Zahran MK. Green synthesis of silver nanoparticles using polysaccharides extracted from marine macro algae. *Carbohydr Polym*. 2013;96(2):403–410. doi:10.1016/j.carbpol.2013.03.071
6. Khalifa E, Rafea MA, Mustapha N, et al. Silver nanoparticles synthesized by probiotic bacteria and antibacterial role in resistant bacteria. *AMB Express*. 2023;13(1). doi:10.1186/s13568-023-01651-7.
7. Santos TS, Silva TM, Cardoso JC, et al. Biosynthesis of silver nanoparticles mediated by entomopathogenic fungi: antimicrobial resistance, nanopesticides, and toxicity. *Antibiotics-Basel*. 2021;10(7):1
8. Mahyoub JA. Bioactivity of two marine algae extracts and their synthesized silver nanoparticles as safe controls against Musca domestica housefly. *Entomo Res*. 2021;51(7):323–330. doi:10.1111/1748-5967.12512
9. Mohammed AE, Al-Qahtani A, Al-Mutairi A, et al. Antibacterial and cytotoxic potential of biosynthesized silver nanoparticles by some plant extracts. *Nanomaterials*. 2018;8(6):382. doi:10.3390/nano8060382
10. Liu X, Chen J, Yang W, et al. Biosynthesis of silver nanoparticles with antimicrobial and anticancer properties using two novel yeasts. *Sci Rep*. 2021;11(1):1.
11. Banihashem SM, Moradi A, Evazzadeh B, et al. Biogenically synthesized nanoparticles in wastewater treatment; a greener approach: a review. *Clean Technol Environ Policy*. 2024;26(6):1731–1754. doi:10.1007/s10098-023-02720-y
12. Roy A, Bulut O, Some S, et al. Green synthesis of silver nanoparticles: biomolecule-nanoparticle organizations targeting antimicrobial activity[J]. *RSC Adv*. 2019;9(5):2673–2702. doi:10.1039/C8RA08982E
13. Devasvaran K, Alallam B, Lee C, et al. Clinacanthus nutans crude polysaccharide extract as a green platform for microwave-assisted synthesis of silver nanoparticles: optimization, characterization, and evaluation of bioactivities. *Int J Biol Macromol*. 2024;278;134893 doi:10.1016/j.ijbiomac.2024.134893
14. Wang G, Yang X, Chen X, et al. Construction and antibacterial activities of walnut green husk polysaccharide based silver nanoparticles (AgNPs). *Int J Biol Macromol*. 2024;276;133798 doi:10.1016/j.ijbiomac.2024.133798.
15. Ma Z, Liu J, Liu Y, et al. Green synthesis of silver nanoparticles using soluble soybean polysaccharide and their application in antibacterial coatings. *Int J Biol Macromol*. 2021;166:567–577. doi:10.1016/j.ijbiomac.2020.10.214
16. Yang X, Niu Y, Fan Y, et al. Green synthesis of Poria cocos polysaccharides-silver nanoparticles and their applications in food packaging. *Int J Biol Macromol*. 2024;269;131928 doi:10.1016/j.ijbiomac.2024.131928
17. Li H, Pan Z, Chen J, et al. Green synthesis of silver nanoparticles using Phlebopus portentosus polysaccharide and their antioxidant, antidiabetic, anticancer, and antimicrobial activities. *Int J Biol Macromol*. 2024;254;127579 doi:10.1016/j.ijbiomac.2023.127579
18. Hu YF, Zhou D, Zeng QN, et al. Optimization of enzymatic hydrolysis process, structural characterization and antioxidant activity analysis of Gastrodia elata polysaccharide. *Sci Technol Food Ind*. 2025;46: 1–10 doi:doi:10.13386/j.issn1002-0306.2024030247
19. Gao X, Qi J, Ho CT, et al. Structural characterization and immunomodulatory activity of a water-soluble polysaccharide from Ganoderma leucocontextum fruiting bodies. *Carbohydr Polym*. 2020;249:116874. doi:10.1016/j.carbpol.2020.116874
20. Zhang HH, Li C, Liu HP, et al. Extraction and purification of Cinnamomum cassia polysaccharides and its antioxidant and hypoglycemic activities in vitro. *Sci Technol Food Ind*. 2024;45(07):15–24.
21. Zhao S, Han Z, Yang L, et al. Extraction, characterization and antioxidant activity evaluation of polysaccharides from Smilacina japonica. *Int J Biol Macromol*. 2020;151:576–583. doi:10.1016/j.ijbiomac.2020.02.015
22. Li G, Chen P, Zhao Y, et al. Isolation, structural characterization and anti-oxidant activity of a novel polysaccharide from garlic bolt. *Carbohydr Polym*. 2021;267:118194. doi:10.1016/j.carbpol.2021.118194
23. Wang J, Xu J, Zhang J, et al. Physicochemical properties and antioxidant activities of polysaccharide from floral mushroom cultivated in Huangshan Mountain. *Carbohydr Polym*. 2015;131:240–247. doi:10.1016/j.carbpol.2015.05.052
24. Chen W, Zhu X, Ma J, et al. Structural Elucidation of a novel pectin-polysaccharide from the petal of Saussurea laniceps and the mechanism of its anti-HBV activity. *Carbohydr Polym*. 2019;223:115077. doi:10.1016/j.carbpol.2019.115077
25. Zha XQ, Lu CQ, Cui SH, et al. Structural identification and immunostimulating activity of a Laminaria japonica polysaccharide. *Int J Biol Macromol*. 2015;78:429–438. doi:10.1016/j.ijbiomac.2015.04.047
26. Ji X, Yan Y, Hou C, et al. Structural characterization of a galacturonic acid-rich polysaccharide from Ziziphus jujuba cv. Muzao. *Int J Biol Macromol*. 2020;147:844–852. doi:10.1016/j.ijbiomac.2019.09.244
27. Chen G, Jiang N, Zheng J, et al. Structural characterization and anti-inflammatory activity of polysaccharides from Astragalus membranaceus. *Int J Biol Macromol*. 2023;241:124386. doi:10.1016/j.ijbiomac.2023.124386

28. Wang ZB, Pei JJ, Ma HL, et al. Effect of extraction media on preliminary characterizations and antioxidant activities of Phellinus linteus polysaccharides. *Carbohydr Polym*. 2014;109:49–55. doi:10.1016/j.carbpol.2014.03.057
29. Zhang H, Zou P, Zhao H, et al. Isolation, purification, structure and antioxidant activity of polysaccharide from pinecones of Pinus koraiensis. *Carbohydr Polym*. 2021;251:117078. doi:10.1016/j.carbpol.2020.117078
30. Wu J, Zhang F, Zhang H. Facile synthesis of carboxymethyl curdlan-capped silver nanoparticles and their application in SERS. *Carbohydr Polym*. 2012;90(1):261–269. doi:10.1016/j.carbpol.2012.05.033
31. Wang L, Tian Y, Zhang P, et al. Polysaccharide isolated from Rosa roxburghii Tratt fruit as a stabilizing and reducing agent for the synthesis of silver nanoparticles: antibacterial and preservative properties. *J Food Measure Charac*. 2022;16(2):1241–1251. doi:10.1007/s11694-021-01248-3
32. Kaplan O, Tosun NG, Ozgur A, et al. Microwave-assisted green synthesis of silver nanoparticles using crude extracts of Boletus edulis and Coriolus versicolor: characterization, anticancer, antimicrobial and wound healing activities. *Journal of Drug Delivery Science and Technology*. 2021;64:102641. doi:10.1016/j.jddst.2021.102641
33. Djahaniani H, Rahimi-Nasrabadi M, Saiedpour M, et al. Facile synthesis of silver nanoparticles using Tribulus longipetalus extract and their antioxidant and antibacterial activities. *Int J Food Prop*. 2017;20(4):922–930. doi:10.1080/10942912.2016.1188826
34. Li S, Zhang Y, Xu X, et al. Triple helical polysaccharide-induced good dispersion of silver nanoparticles in water. *Biomacromolecules*. 2011;12(8):2864–2871. doi:10.1021/bm2001439
35. Saravanan M, Duche K, Asmelash T, et al. "Nano-biomaterials" –A new approach concerning multi-drug resistant tuberculosis (MDR-TB). *Pharma Nanotechnol*. 2015;3(1):5–18. doi:10.2174/2211738503666150415230743
36. Yun'An Q, Lin C, Ruiyan L, et al. Potential antibacterial mechanism of silver nanoparticles and the optimization of orthopedic implants by advanced modification technologies. *Int J Nanomed*. 2018;13:3311–3327. doi:10.2147/IJN.S165125
37. Talib H, Mehmood A, Amjad MS, et al. Antibacterial, antioxidant, and anticancer potential of green fabricated silver nanoparticles made from *Viburnum grandiflorum* leaf extract. *Bot Stud*. 2024;65(1). doi:10.1186/s40529-024-00411-5.
38. Xiong ZX, Cui KP, Chen C, et al. The effects of silver particle size on bacterioplankton community and potential function in aquatic environment. *J Environ Chem Eng*. 2024;12(2):112012. doi:10.1016/j.jece.2024.112012
39. Agnihotri S, Mukherji S, Mukherji S. Size-controlled silver nanoparticles synthesized over the range 5-100 nm using the same protocol and their antibacterial efficacy. *RSC Adv*. 2014;4(8):3974–3983. doi:10.1039/C3RA44507K
40. Zhou W, Jia Z, Xiong P, et al. Bioinspired and biomimetic AgNPs/gentamicin-embedded silk fibroin coatings for robust antibacterial and osteogenetic applications. *ACS Appl Mater Interfaces*. 2017;9(31):25643–26630. doi:10.1021/acsami.7b06757
41. Alcantara MTS, Lincopan N, Santoset PM, et al. Simultaneous hydrogel cross linking and silver nanoparticle formation by using ionizing radiation to obtain antimicrobial hydrogels. *Radiat Phys Chem*. 2020;169:108777. doi:10.1016/j.radphyschem.2020.108777
42. Hongal AM, Shettar AK, Hoskeri JH, et al. Silver nanoparticles mediated apoptosis and cell cycle arrest in lung cancer A549. *3 Biotech*. 2024;14(1). doi:10.1007/s13205-024-04064-w.
43. Niluxsshun MKD, Masilamani K, Mathiventhan U. Green synthesis of silver nanoparticles from the extracts of fruit peel of *Citrus tangerina,Citrus sinensis*, and *Citrus limon* for antibacterial activities. *Bioinorganic Chem Appl*. 2021;2021:1–8. doi:10.1155/2021/6695734
44. Devasvaran K, Alallam B, Yunus MA, et al. Microwave-assisted green synthesis of silver nanoparticles using alkaline extracted crude polysaccharide of *C. Nutans*: optimisation, characterisation, toxicity, anticancer potential and antibacterial studies. *J Drug Delivery Sci Technol*. 2023;86;104688. doi:10.1016/j.jddst.2023.104688.
45. Chakraborty B, Bhat M, Basavarajappa DS, et al. Biosynthesis and characterization of polysaccharide-capped silver nanoparticles from *Acalypha indica* L. and evaluation of their biological activities. *Environ Res*. 2023;225:115614. doi:10.1016/j.envres.2023.115614
46. Al-Badwy AH, Khalil AM, Bashal AH, et al. Polysaccharides from *Spirulina platensis* (PSP): promising biostimulants for the green synthesis of silver nanoparticles and their potential application in the treatment of cancer tumors. *Microb Cell Fact*. 2023;22(1):247. doi:10.1186/s12934-023-02257-1